Microstructural effects on the dynamical relaxation of glasses and glass composites: A molecular dynamics study

Guo-Jian Lyu, Ji-Chao Qiao, Yao Yao, Yun-Jiang Wang, Julien Morthomas, Claudio Fusco, David Rodney

Microstructural effects on the dynamical relaxation of glasses and glass composites: a molecular dynamics study

Authors: Guo-Jian Lyu[a,b,c]*, Ji-Chao Qiao[c], Yao Yao[c,d], Yun-Jiang Wang[a], Julien Morthomas[b]*, Claudio Fusco[b]*, David Rodney[e]*

[a]State Key Laboratory of Nonlinear Mechanics, Institute of Mechanics, Chinese Academy of Sciences, Beijing 100190, China

[b]Univ Lyon, INSA Lyon, UCBL, CNRS, MATEIS, UMR5510, 69621 Villeurbanne , France

[c]School of Mechanics, Civil Engineering Architecture, Northwestern Polytechnical University, Xi'an 710072, P. R. China

[d]School of Civil Engineering, Xi'an University of Architecture and Technology, Xi'an 710055, China

[e]Institut Lumière Matière, UMR5306 Université Lyon 1-CNRS, Université de Lyon, F-69622 Villeurbanne Cedex, France

*Corresponding authors:
Dr. Guo-Jian Lyu
E-mail address: lyuguojian@imech.ac.cn

Dr. Julien Morthomas
E-mail address: julien.morthomas@insa-lyon.fr

Dr. Claudio Fusco
E-mail address: claudio.fusco@insa-lyon.fr

Prof. David Rodney
E-mail address: David.rodney@univ-lyon1.fr

Abstract

One way to increase the ductility of metallic glasses is to induce heterogeneous microstructures, as for example in nanoglasses and crystal-glass composites. The heterogeneities have important consequences not only on the development of shear bands, but also on the structural relaxations in the glass phase. Experiments using dynamical mechanical spectroscopy (DMS) have been conducted, but an atomic-scale picture is still lacking. Here we apply DMS within molecular dynamics simulations to a classical CuZr metallic glass to study how structural relaxations and mechanical energy dissipation are affected by different microstructures, including nanoglasses, crystal-glass nanolaminates and glasses with spherical crystalline inclusions. We find that in a fully glassy system, not only the fraction but also the spatial homogeneity of "hard" icosahedral environments matter. When hard crystalline particles are introduced, the storage modulus simply results from volumetric averages consistent with the classical Voigt and Reuss bounds. On the other hand, loss moduli are much more complex and can be smaller or larger than in a pure glass depending on the microstructure and loading condition. Atomistic processes leading to these evolutions are discussed and remaining open questions are highlighted.

Keywords: Metallic glasses; Composites; Nanoglass; Dynamic Mechanic spectrum; Interfaces

1 Introduction

Metallic glasses are a classical example of 'strong-yet-brittle' materials [1]. A general strategy to, at least, delay their brittle failure is to create a microstructure that can impede the development of an unstable shear band. One successful approach has been to design composites, with a crystalline phase embedded in the glass matrix [2–4]. The crystalline phase may be ex-situ or in-situ. In the former case, crystalline fibers [5] or laminates [6] were incorporated into a glassy matrix. In the latter case, crystalline dendrites [2,3,7–10] or more spherical precipitates [11] were obtained by a partial crystallization of the glass. Careful optimization of the process parameters allows to significantly increase the toughness and tensile ductility, while retaining a high tensile strength [12]. Another successful way to induce microstructural heterogeneities is to produce nanoglasses, by consolidating nanometer-sized glassy particles [13–16].

In-situ composites particularly studied both in experiments [11,17–21] and simulations [22–25] are CuZr-based metallic glasses with a B2-CuZr crystalline phase. In-situ crystallites are near spherical and show transformation-induced plasticity with a shape memory effect, leading to large plastic deformability and pronounced work hardening [26–28].

So far, most of the attention has been on the mechanical properties of metallic glass matrix composites for structural engineering purposes, i.e. on the yield stress and fracture toughness. However, glasses are also characterized by complex structural relaxation processes [29,30] that are bound to be affected by crystalline phases, particularly at the nanoscale. Relaxation processes are best studied using dynamical mechanical spectroscopy (DMS) [31,32]. DMS is a convenient and useful tool to characterize viscoelasticity and relaxation properties of amorphous materials, as it can detect the structural changes at a molecular or atomic scale for wide temperature and frequency ranges. In pure glasses, several peaks have been observed in both experiments [33] and simulations [34]. The α-relaxation is the main relaxation mode, directly related to viscous flow and the glass transition. At lower temperature, a secondary β-relaxation is observed, intimately related to plasticity [35–37] and connected to string-like events through molecular dynamics simulations [38,39]. Other peaks, i.e., the γ-relaxation [40] and anomalous α_2 relaxation [41], have also been reported. Much less is known about relaxation processes in metallic glass matrix composites. So far, DMS has been applied experimentally to in-situ and ex-situ glassy composites, leading to a wealth of processes, due either to the release of internal stresses during DMS heating [42] or to solid-state transformations (phase transformation, precipitation) of the crystalline phase leading to new peaks [43–45], to the doubling of existing peaks [42,46] or to weakened, broadened and shifted relaxation peaks induced by doping [47]. The atomic-scale mechanisms controlling microstructural effects on dissipation remain however unknown.

In this work, we perform Molecular Dynamics (MD) simulations of dynamical mechanical spectroscopy (MD-DMS) to study the effect of different microstructures on the relaxation and viscoelasticity of glass composites and nanoglasses. We consider a classical CuZr glass with B2-CuZr crystallites, which we deform cyclically, either longitudinally or by shear. The same MD-DMS technique has been applied to study pure glasses [34,41,48,49]. Here, to investigate the effect of a microstructure, we modelled several systems of varying complexity: pure glasses quenched at different rates, glass-glass nanocomposites as well as crystal-glass composites with B2-CuZr crystallites of different geometries representative of either in-situ (spherical precipitates), ex-situ (nanolaminates) and more intricate (interconnected gyroid phases) composites.

2 Methodology

All the simulations were conducted using the open source LAMMPS package [50]. A Finnis-Sinclair type Cu-Zr embedded atom method (EAM) potential developed by Mendelev et al. was used to describe interatomic interactions [51]. This potential has been used many times in the past to study the properties of CuZr metallic glasses, including the formation and interaction of shear bands [52], the brittle-to-ductile transition [53], as well as the aging and rejuvenation under cyclic deformation [54]. This potential was also recently used by the present authors to study the dynamic correspondence principle in pure glasses [48]. Nosé-Hoover thermostat and barostat were applied during the entire preparation protocol for all glasses and glassy composites. Atomic visualizations were performed using Ovito [55].

As sketched in Fig. 1, to produce the crystal-glass composites, we start by generating $Cu_{64}Zr_{36}$ metallic glasses by quenching a $Cu_{64}Zr_{36}$ liquid from 2000 K to 100 K at 10^{11} K/s at zero pressure. The dimensions of glasses are about 11.9 nm × 11.9 nm × 11.9 nm, containing 108,000 atoms. As expected and illustrated in Fig. 2(a), a clear deviation during cooling can be observed in the linear curve of averaged atomic volume, corresponding to a glass transition with a glass-transition temperature (T_g) of about 800 K. As illustrated in Fig. 1(a), to produce pure glass structures for DMS deformation while mimicking the experimental DMS process, the glass was heated again to each target temperature at a heating rate of 10^{12} K/s, and 15 configurations (blue dots in Fig. 1(a)) with a temperature interval of 100 K were generated for subsequent 1 ns-annealing (red dots in Fig. 1(a)) and DMS deformations. For a better understanding of the kinetic behavior around the glass transition, atomic configurations extracted during heating at temperatures between 600 K to 1100 K were annealed for 40 ns. The result is shown in Fig. 2(b). The potential energy remains constant at 1000 K and 1100 K indicating that the samples are in an equilibrated liquid state. At the lowest temperatures (600 and 700 K), the energy variation is slow, due to kinetically-limited aging of the glassy state. In-between (800

and 900 K), the potential energy first increases rapidly to reach the same level as during cooling, then remains almost constant for about 2 ns, before decreasing dramatically as annealing takes place. High temperatures near the glass-transition temperature allow for an accelerated aging resulting in low energy glasses as already demonstrated by Derlet et al. [56].

As shown in Fig. 1(b), to obtain the composite structures, atoms in specific regions of the glass were replaced with B2-CuZr crystals after the initial cooling and a 1 ns-annealing at 100 K. The crystal directions [100], [010] and [001] of B2-CuZr were set along the X, Y and Z axes of simulation box. In this work, composites with geometries of spheres, laminates and gyroids [57] were investigated, as illustrated in Fig. 1(c). After insertion of B2-CuZr crystals, all composites were heated to 800 K at 10^{12} K/s and annealed for 1 ns to relax the glass-crystalline interface, and finally cooled back down to 100 K at 10^{12} K/s. Similar to the pure glass, 15 configurations were then extracted at 100 K intervals during a 10^{12} K/s-heating and annealed for 1 ns before being tested by MD-DMS.

To study the effect of an internal microstructure in a glass, we also generated nanoglasses using the Poisson-Voronoi tessellation method [58]. Each nanograin was taken from the original 10^{11} K/s quenched $Cu_{64}Zr_{36}$ glass with a random orientation at 100 K, corresponding to the green dot in Fig. 1(b). The sample was first energy minimized to avoid atomic overlaps inside the glass-glass interfaces. A hydrostatic pressure of 1.5 GPa was then applied for 1 ns at 100 K to eliminate the voids near the interfaces, then followed by another 1 ns-annealing at 100 K. The reason for not annealing at 800 K is to avoid eliminating the artificial glass-glass interfaces due to fast atomic diffusion. The subsequent procedures before MD-DMS simulations are the same as with the pure glass and crystal-glass composites.

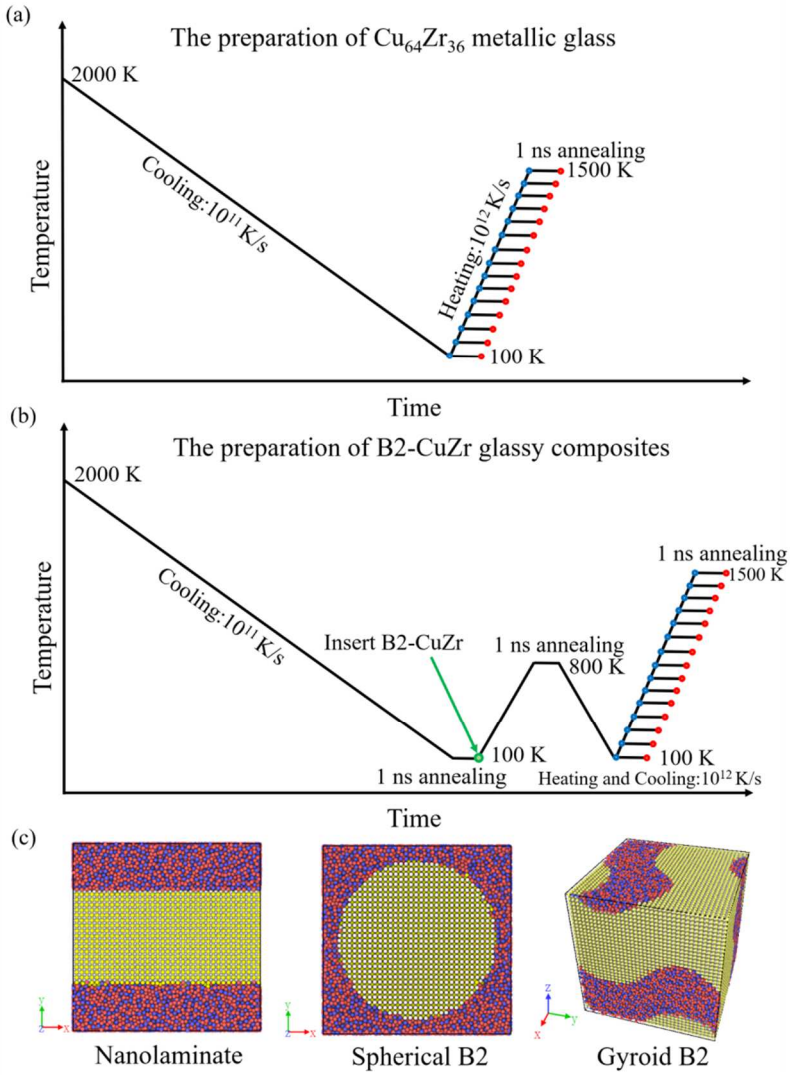

Fig. 1 (a-b) Protocols to produces $Cu_{64}Zr_{36}$ metallic glasses and B2-CuZr glassy composites, respectively; (c) Examples of atomic configurations of a nanolaminate, a spherical and a gyroid B2 composite. Red and blue atoms are Cu and Zr atoms in the glass phase; yellow and white atoms are Cu and Zr atoms in the B2-CuZr crystals.

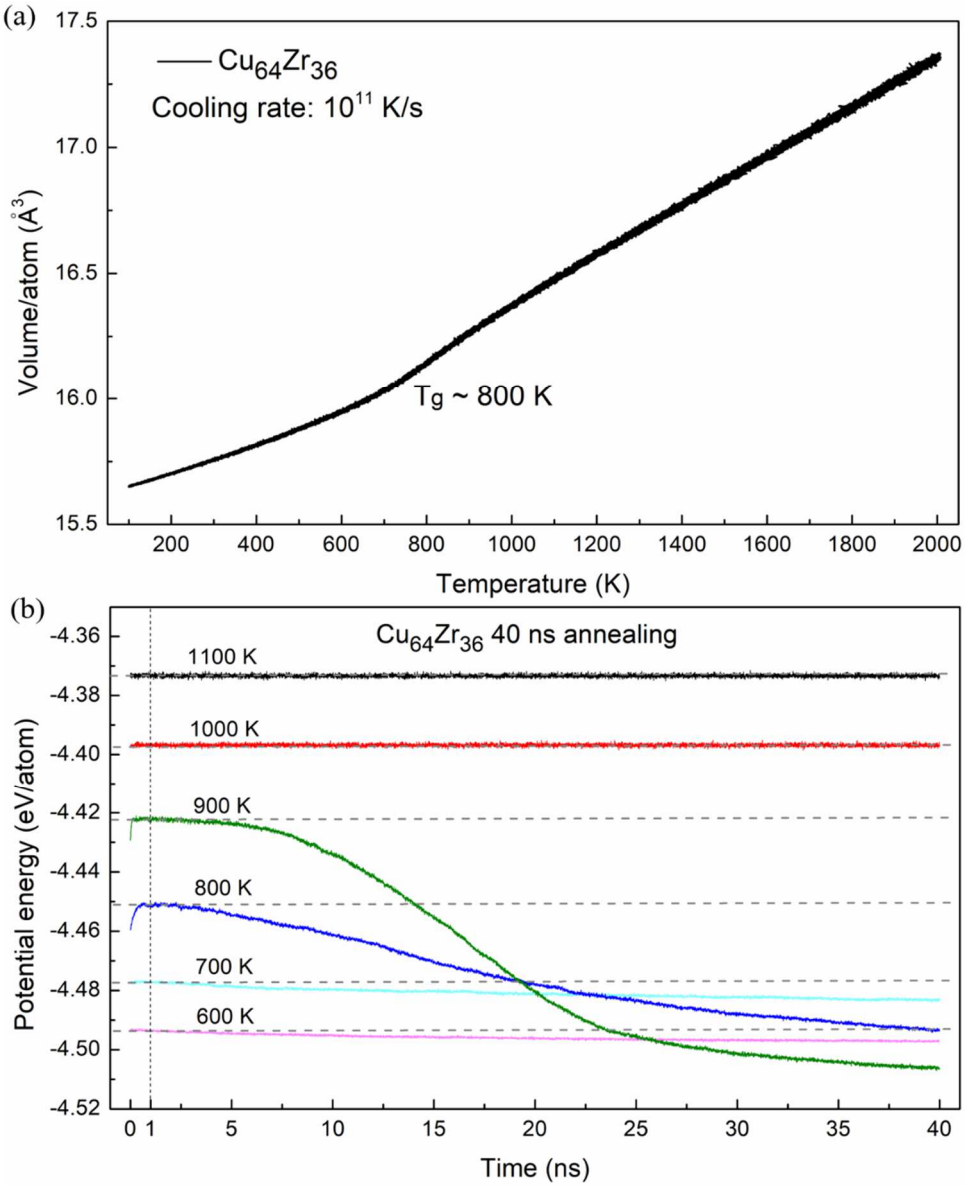

Fig. 2 (a) Averaged atomic volume while cooling a liquid from 2000 K to 100 K; (b) Atomic potential energy as a function of annealing time at different temperatures.

The MD-DMS method proposed by Yu et al. [34] was used in this work. In order to obtain the complex moduli, for instance the complex longitudinal moduli M^*, a strain $\varepsilon_{xx}(t) = \varepsilon_A \sin(\omega t)$ was applied along the X direction while holding the Y and Z dimensions fixed, with ε_A the strain amplitude and $f = \omega/2\pi$ the deformation frequency. During the MD-DMS deformation, a Nosé-Hoover thermostat was applied to keep the temperature constant. The resulting stress was then fitted as $\sigma_{xx}(t) = \sigma_0 + \sigma_A \sin(\omega t + \delta)$, with σ_A the stress amplitude and δ the phase shift. The complex longitudinal modulus is given as $M^* = (\sigma_A/\varepsilon_A)[\cos(\delta) + i\sin(\delta)]$, with a real part, i.e. the storage modulus, $M' = (\sigma_A/\varepsilon_A)\cos(\delta)$ and an imaginary part, i.e. the loss modulus, $M'' = (\sigma_A/\varepsilon_A)\sin(\delta)$. Details for DMS deformation procedures can be found in our previous work [48]. In the current work, only the

complex longitudinal modulus M^* and shear modulus G^* are considered, which suffices to know all storage and loss moduli for the pure glass, thanks to the dynamic correspondence principle [48]. We used a reference deformation frequency of 10 GHz, with a strain amplitude of 2.5%, well within the static elastic regime of the glasses in MD simulations. To limit statistical errors, each data was averaged over 5 deformation cycles. The cyclic deformation was thus applied for a total of 0.5 ns, short enough to avoid aging of glass, even near the glass transition temperature, as seen in Fig. 2(b).

3 Results

3.1 Pure glasses and nanoglasses

Cu-centered icosahedral clusters are the dominant structural motif in CuZr glasses. As extensively investigated in the literature [59–61], they form stable atomic configurations, with a relatively high local atomic packing density and a high shear resistance. Under deformation, they form a rigid backbone, which deforms mostly elastically. As a result, their density has been shown anticorrelated with energy dissipation [34,48,62], i.e. the more Cu-centered icosahedral clusters in the glass, the less energy dissipation. Other types of clusters, typically considered as "geometrically unfavored motifs" (GUM) [63–65] or "soft regions", are loosely packed and undergo irreversible rearrangements, which contribute to energy dissipation [48]. To obtain structures with varying fractions of Cu-centered icosahedral environments, a classical method is to change the cooling rate, since a higher cooling rate results in a lower fraction of icosahedral clusters. Another way is to generate a nanoglass, since the highly perturbed glass-glass interfaces will contain very low fractions of icosahedral clusters.

In this section, we designed three types of $Cu_{64}Zr_{36}$ metallic glasses with different fractions of Cu-centered icosahedral clusters: two pure glasses generated with cooling rates of 10^{11} K/s and 10^{12} K/s, and a nanoglass constructed from the 10^{11} K/s quenched glass. Fig. 3(a) illustrates the atomic structure of the nanoglass composed of 14 grains with periodic boundary conditions. Fig. 3(b) shows only the Cu atoms at the center of icosahedral clusters, illustrating that there are no such atoms near the glass-glass interfaces. As explained above, we prepared 15 configurations from both initial glasses and from the nanoglass to perform MD-DMS. Fig. 3(c) shows the initial fraction of Cu-centered icosahedral clusters. We see that at low temperatures, the most slowly quenched glass has the highest fraction of icosahedral clusters, while the most rapidly quenched glass has the lowest fraction. The nanoglass is in-between. At higher temperatures, the difference between the different systems decreases and above the glass-transition temperature (T_g=800 K), all systems are equivalent, which is expected since they are all in the liquid state.

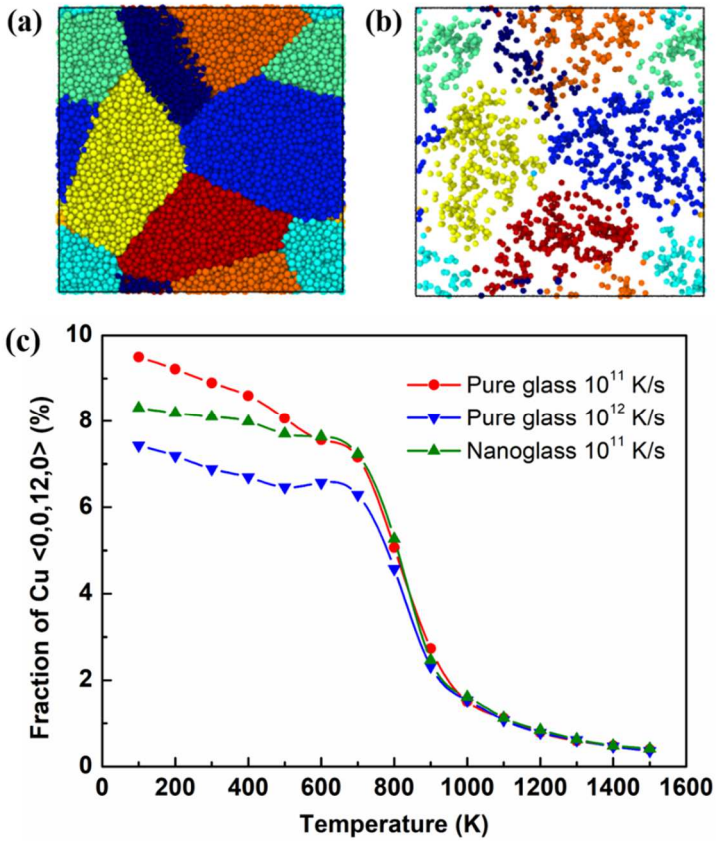

Fig. 3 (a) Atomic structure of a $Cu_{64}Zr_{36}$ nanoglass and (b) Cu-<0,0,12,0> atoms in the nanoglass; (c) Temperature dependence of the fraction of Cu-<0,0,12,0> atoms in a slowly- and a rapidly-quenched glass as well as in a nanoglass.

We conducted MD-DMS simulations on the three glasses. Fig. 4 presents the measured complex longitudinal moduli M^* and complex shear moduli G^*. Both M'' and G'' present a marked relaxation peak at the glass transition temperature (T_g=800 K), above which all samples are in the liquid state where they have lost the memory of their initial state and thus show identical properties. Below 800 K, both glasses and the nanoglass have similar longitudinal storage moduli M' while in shear, G' is slightly larger for the slowly quenched glass than for the rapidly quenched glass and the nanoglass. The microstructure has a stronger effect on the loss moduli. First, we recover that the rapidly quenched glass has larger M'' and G'' than the slowly quenched glass, which is consistent with the lower density of icosahedral clusters in the former than in the latter. More surprising is the fact that the nanoglass, despite having a density of icosahedral clusters in-between both glasses, has the highest loss modulus. The reason can be found in Fig. 5, in which we show the residual atomic displacements at the end of each loading cycle both on the surface and in the interior of a representative nanograin. We see that the residual atomic displacements are mainly concentrated in the glass-glass interfaces and are close to zero in the interior of the grain. Since the global strain returns back to zero at the end

of each loading cycle, the residual atomic displacements visible in the interface are irreversible atomic rearrangements, which increase the energy dissipation.

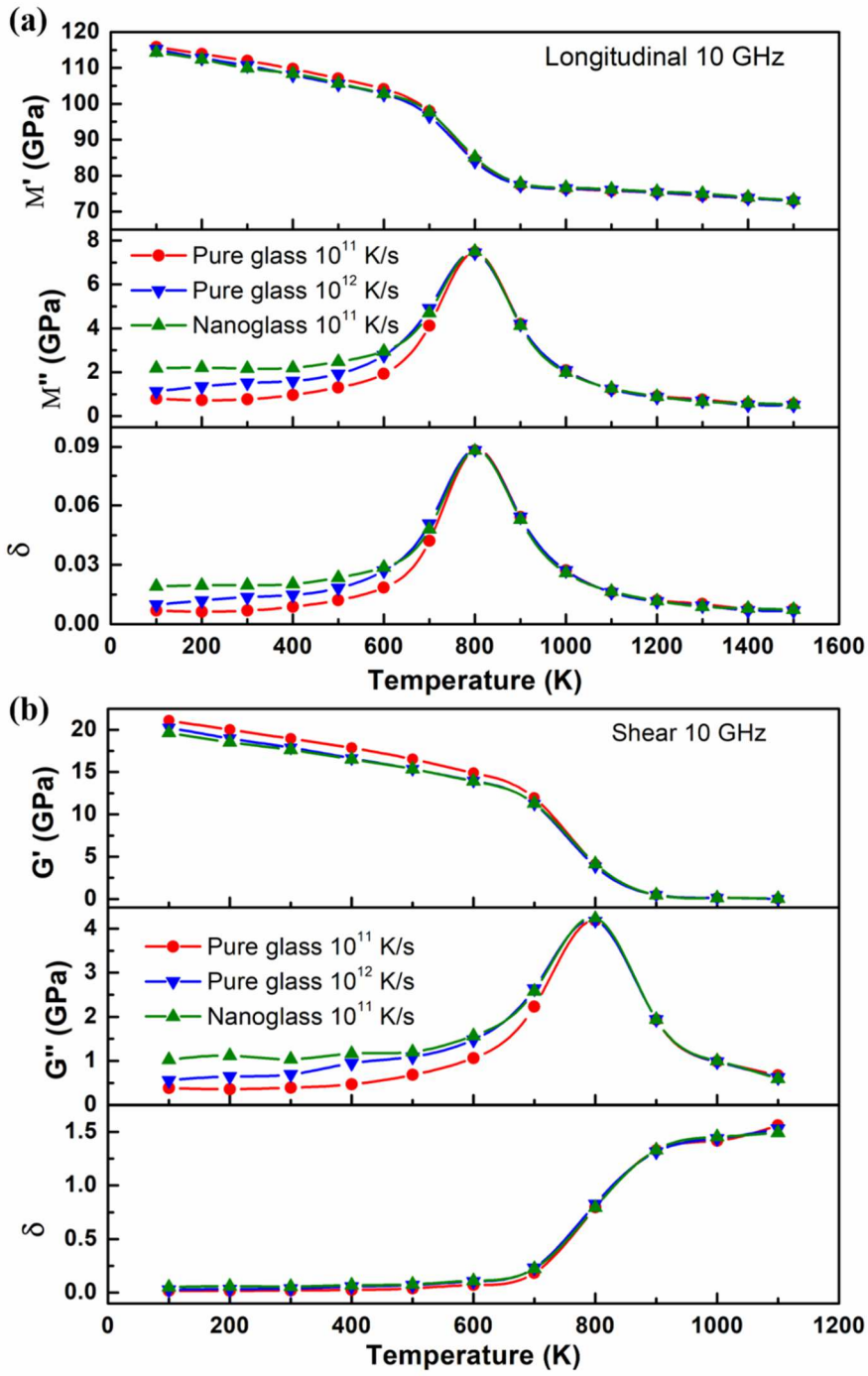

Fig. 4 (a) Complex longitudinal moduli M^* and (b) shear moduli G^* of different metallic glasses: CuZr glass with cooling rates of 10^{11} K/s and 10^{12} K/s and a CuZr nanoglass.

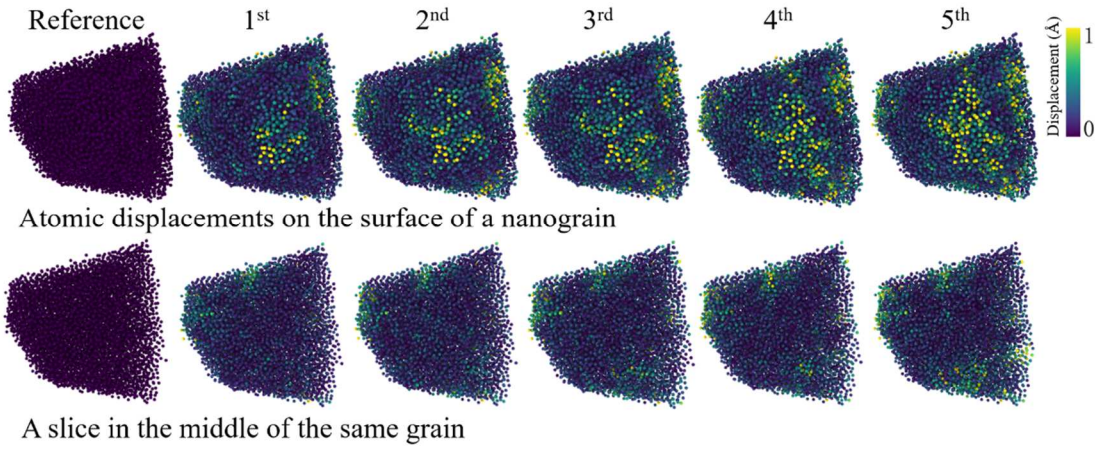

Fig. 5 Atomic displacements at the end of each loading cycle on the surface of a nanograin (upper figures) and in a slice in the middle of the same grain at 100 K (bottom figures) under longitudinal deformation.

This first set of glassy systems shows that not only the density of icosahedral clusters but also the localized deformation within the glass-glass interfaces affects energy dissipation. The nanoglass has a higher density of clusters than the rapidly quenched glass (10^{12} K/s) but has also a higher dissipation at low temperatures because the glass-glass interfaces are localized "soft" regions prone to irreversible atomic rearrangements. Icosahedral clusters may also be destroyed in the course of the deformation, which will further increase the dissipation. By way of contrast, icosahedral clusters are less dense in the rapidly quenched glass but they are homogeneously distributed and thus still limit atomic rearrangements. Therefore, the glass-glass interfaces play an important role in the dynamic mechanical response by creating non-icosahedral environments in nanoglasses.

In the case of a nanoglass, we introduced "soft" regions in a pure glass. We now consider the opposite case, where we introduce "strong" crystalline regions in the glass.

3.2 Nanolaminates

The first crystal-glass composite to be considered is a nanolaminate made of 50% $Cu_{64}Zr_{36}$ glass, 50% B2-CuZr crystal. Since this structure is not isotropic, we need to distinguish different directions of loading illustrated in Fig. 6. For longitudinal deformations, the cyclic deformation can be applied either perpendicularly (Y) or parallel (X) to the glass-crystal interface, which are denoted as iso-stress and iso-strain longitudinal loadings, respectively. Similarly, two cyclic shear deformations can be applied, in planes either perpendicular (XY) or parallel (XZ) to the interface, hereinafter denoted as iso-stress and iso-strain shear loadings, respectively. For the iso-stress longitudinal loading (Fig. 6(a)), both phases are subjected to the same applied stress in the Y direction, while the lateral dimensions are fixed. By way of

contrast, with the iso-strain longitudinal loading (Fig. 6(c)), the glass and crystalline phases are compressed or stretched equally in the X direction with the Y and Z dimensions fixed. The cases of iso-stress (Fig. 6(b)) and iso-strain ((Fig. 6(d)) shear loadings are similar. Due to the different elastic moduli of the glass and B2-CuZr crystal, when subjected to the same stress, both phases undergo different strains, and inversely, under the same strain, they develop different stresses.

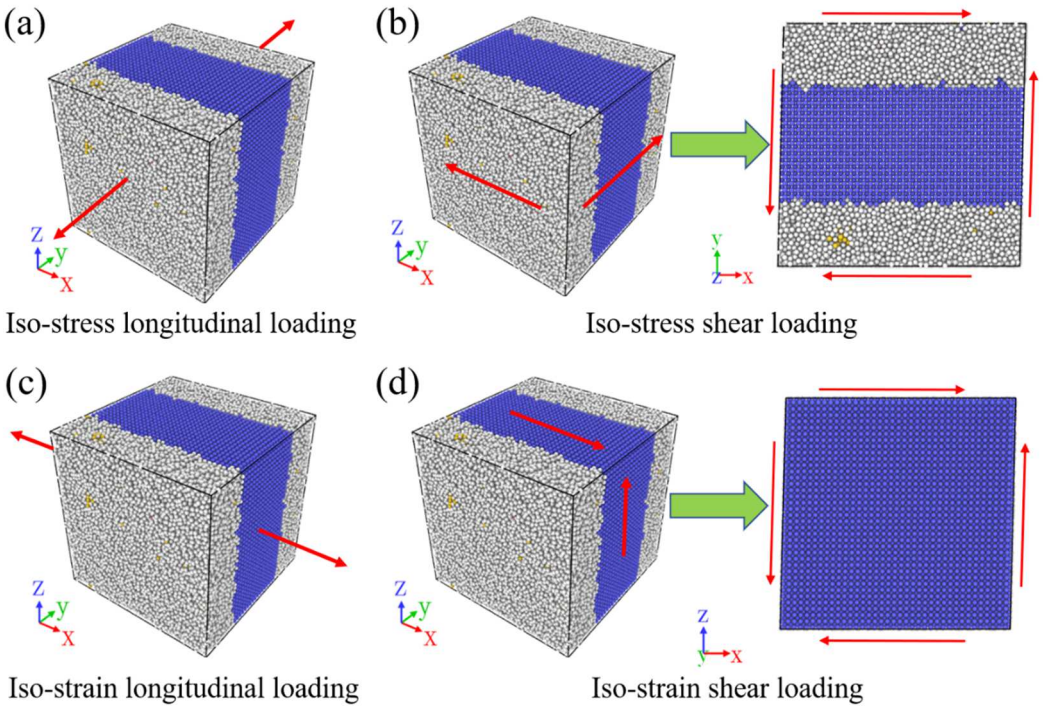

Fig. 6 Loading modes of a glass-crystal nanolaminate composite: (a) iso-stress longitudinal loading with a longitudinal strain applied in the Y direction perpendicular to the laminate interface, (b) iso-stress shear loading with a shear strain applied in the XY plane perpendicular to the laminate interface, (c) iso-strain longitudinal loading with a longitudinal strain in the X direction parallel to the interface, (d) iso-strain shear loading with a shear strain in the XZ plane parallel to the interface.

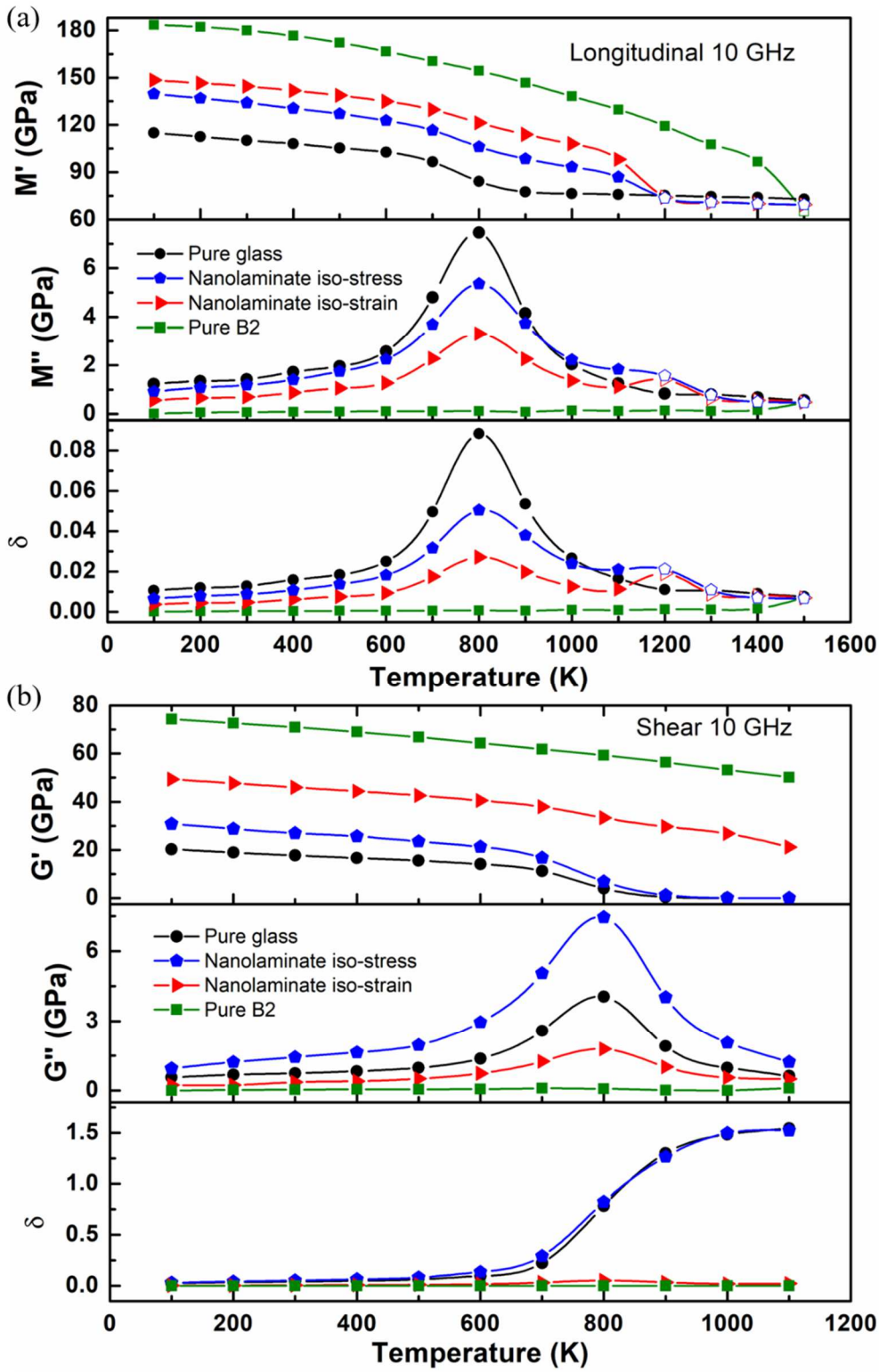

Fig. 7 Complex longitudinal (a) and shear (b) moduli of a 50% crystal- 50% glass nanolaminate composite under iso-stress and iso-strain loadings. Pure glass and pure crystal data are added for comparison. Hollow symbols indicate that the crystalline phase completely disappeared during the cyclic deformation.

Due to the additional heating, cooling and annealing during the preparation of composite samples (see Fig. 1(b)), the structure and mechanical properties of the glass phase may change. To identify more clearly the effect induced by the crystal phase, the pure glasses used in this section as reference were treated with the same thermal processes as the composites.

Fig. 7 (a) presents the complex longitudinal moduli M^* for the pure glass, the pure B2-CuZr crystal and the nanolaminate composite. The pure crystal has as expected a higher storage modulus and an almost zero loss modulus. We therefore expect that, by a simple volumetric effect, adding a crystalline phase in the glass will increase the storage modulus and decrease loss modulus compared to the pure glass. This is precisely what is seen in Fig. 7 (a) for longitudinal loading. Moreover, the storage modulus M' in iso-strain is higher than in iso-stress as expected from the Voigt and Reuss effective moduli discussed in section 4. Conversely, the loss modulus and lag angle are lower in iso-strain than in iso-stress. The case of iso-strain shear shown in Fig. 7 (b) is similar to longitudinal iso-strain, with a higher G' and a lower G'' compared to the pure glass. With iso-strain loading, whether longitudinal or shear, both crystal and glass phases deform equally and the effective modulus of the composite results from a volumetric average of the crystal and glass moduli.

The case of iso-stress shear loading shown in Fig. 7(b) is more complex because G'' is larger than in the pure glass over the entire temperature range. The relaxation peak occurs at the same temperature as in the pure glass (800 K), but has a larger amplitude. With iso-stress loading, the crystal and glass phases are subjected to the same stress but develop different shear strains. Since the glass phase has a much lower G' than the crystal (20 GPa compared to 75 GPa at 100 K), it deforms significantly more. We measured that the strain amplitude at 100 K in the glass phase is close to 4.2% for a 50% crystal-50% glass composite, compared to the overall 2.5% strain amplitude. The strain amplitude in the glass phase also varies with the volume fraction of B2 crystal, i.e., for 20% crystal-80% glass and 80% crystal-20% glass composites at 100 K it is close to 3.0% and 7.0%, respectively. As shown in Fig. 8, the shear loss modulus of a pure glass increases with the strain amplitude. The increase of the strain amplitude in the glass phase due to the presence of the hard crystal phase thus induces an increase of G''. However, the overall increase of the iso-stress shear loss modulus of the nanolaminate seen in Fig.7(b) is larger than in the pure glass in Fig. 8. Moreover, the excess G'' in the composite extends beyond the relaxation peak (Fig.7(b) for T > 800 K) when the glass is in a liquid phase, while the strain amplitude has no effect on the dissipation of the pure glass in the liquid phase (Fig. 8 for T > 800 K). At these high temperatures, the liquid reorganizes quickly, leading to large positive and negative atomic displacements illustrated in Fig. 9(a). However, if we average the X displacements parallel to the laminate interfaces in slabs perpendicular to the Y direction in order to remove the effect of the local rearrangements, we find as shown in Fig. 9(b) that the displacements are discontinuous at the interface at the end of each cycle. This is a signature of sliding, or

shear motion, between the liquid and the glass, which in turn produces dissipation. We therefore conclude that the excess dissipation in the nanolaminate composites with an iso-stress shear loading results from the combined effects of an increased strain amplitude in the glass and shear motions at the crystal-glass interface.

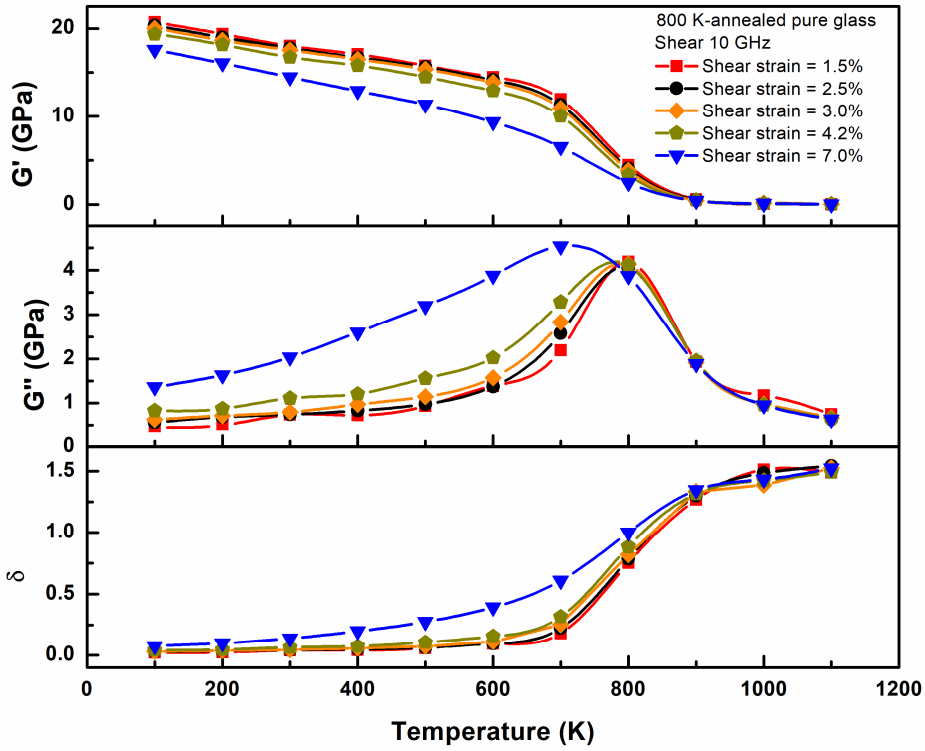

Fig. 8 Complex shear modulus of a pure glass tested with different strain amplitudes noted in the figure. We checked that even at the largest amplitude, the stresses can be accurately fitted by a sinusoid. The values of the shear strains in the legend correspond to the strain amplitudes in the glass phase of sheared nanolaminates with different crystal volume fractions, as explained in the text.

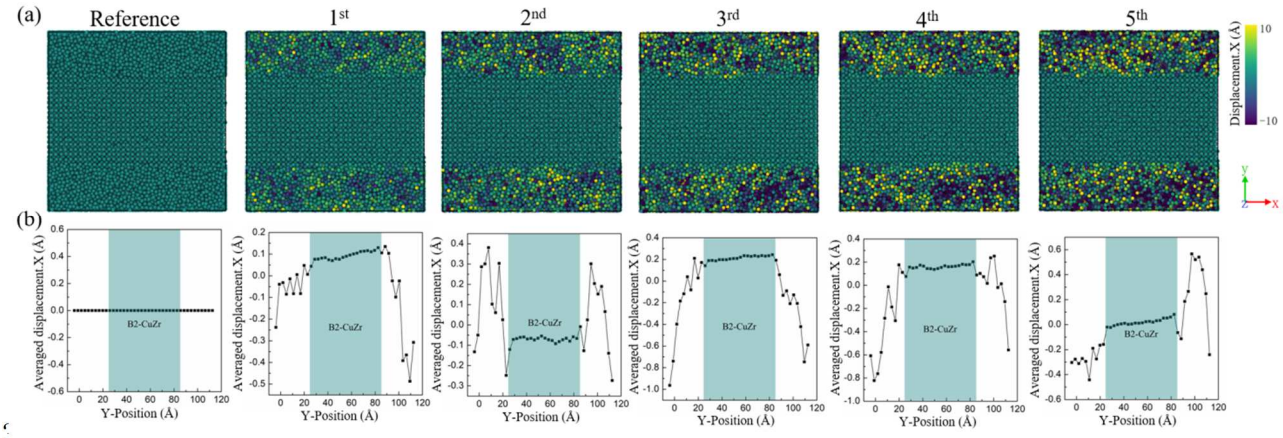

Fig. 9 Non-affine atomic displacements in the X direction at the end of iso-stress shear loading cycles at 1000 K shown (a) with colors in the central Z plane and (b) averaged in slabs perpendicular to the Y direction.

3.3 Spherical B2 composites

We now consider another geometry for the crystal-glass composite, where spherical B2-CuZr crystals are embedded in the glassy matrix. The diameter of the crystalline spheres was varied from 6 nm to 10 nm. As can be seen in Fig. 10, the storage moduli M' and G' again follow an expected volumetric effect and gradually increase as larger B2 spheres are introduced.

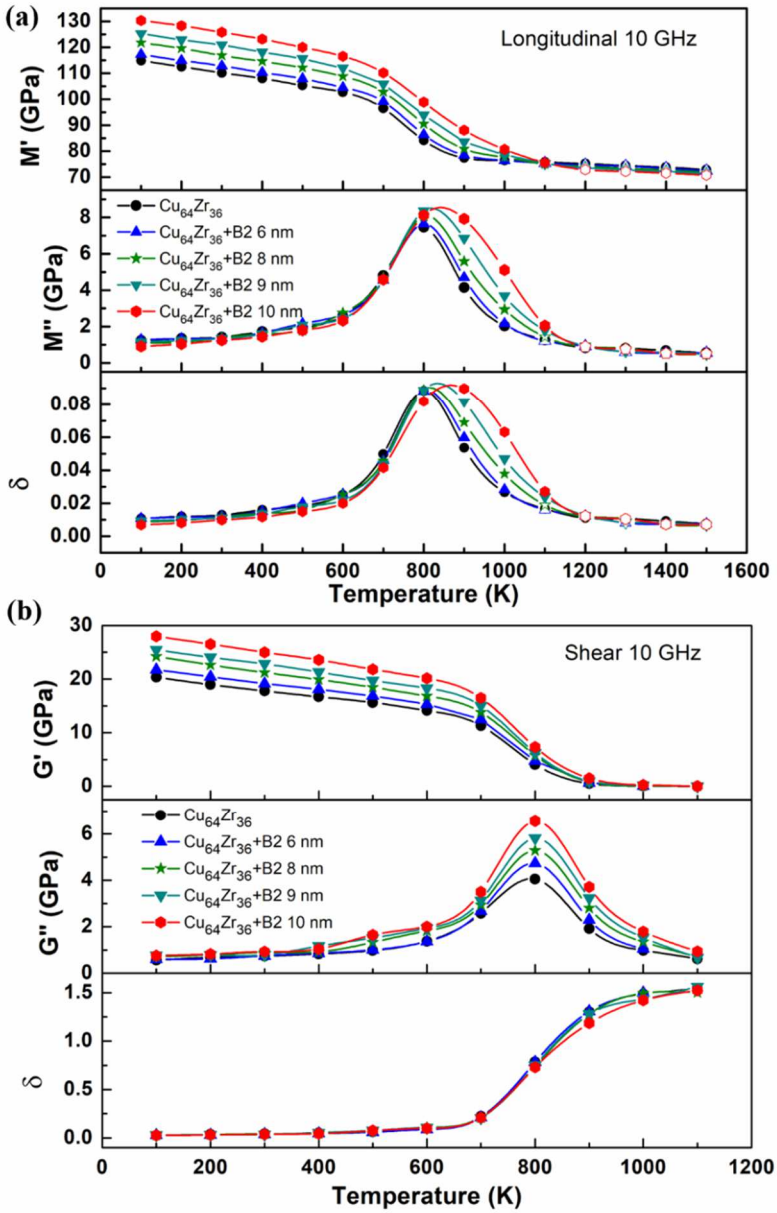

Fig. 10 Complex longitudinal (a) and shear (b) moduli of a composite containing spherical B2-CuZr crystallites of different radii in a glassy matrix. Hollow symbols indicate that the sample completely amorphized during the cyclic deformation.

With spherical inclusions, the stresses and strains are no longer homogeneous in the glassy matrix and the distinction between iso-stress and iso-strain does not apply. However, since the crystalline inclusion is fully embedded in the glassy matrix, crystal and glass phases can deform differently and we should expect a dissipation in the spherical composite closer to the iso-stress rather than the iso-strain nanolaminate. We indeed see in Fig. 10(b) that G'' is larger in the composite than in the pure glass as observed with the iso-stress sheared nanolaminates (Fig. 7(b)). Also, the relaxation peak increases in amplitude but remains at 800 K.

Another observation from Fig. 10(b) is that G'' increases with the sphere radius. We will see below in Fig. 12 that the same is true for iso-stressed nanolaminates. The non-affine displacements shown in Fig. 11 provide an atomistic picture of this behavior. Firstly, we observe a pronounced increase of the atomic displacements near the glass-crystal interface, particularly visible in the heatmaps of Fig. 11(b) generated by averaging the non-affine displacements of Fig. 11(a) on a 30×30 grid in a 1 nm thick slice perpendicular to the Z axis in the middle of the simulation box. The increased non-affine displacements at the interface confirm that the spherical composites behave closer to an iso-stress rather than an iso-strain nanolaminate. Secondly, we see that the atomic displacements at the interface get larger when the size of the spherical inclusion increases due to the larger strain contrast between the two phases, which explains that the dissipation increases as a function of the sphere radius. The case of longitudinal loading shown in Fig. 10(a) is different since we see that M'' hardly depends on the sphere radius before the relaxation peak. In the glassy phase, the presence of spherical crystalline inclusions affects only the storage modulus but not the loss modulus. On the other hand, we see a large effect at high temperatures where the relaxation peak does not increase in amplitude but is shifted towards higher temperatures, with a shift amplitude which increases rapidly with the sphere radius.

This behavior is phenomenologically different from the laminate geometry in Fig. 7 and the shear loading in Fig. 10(b) and implies that the presence of the crystalline spherical inclusions and the interactions between the glass and the crystal stabilize the glassy phase and increases the glass transition temperature.

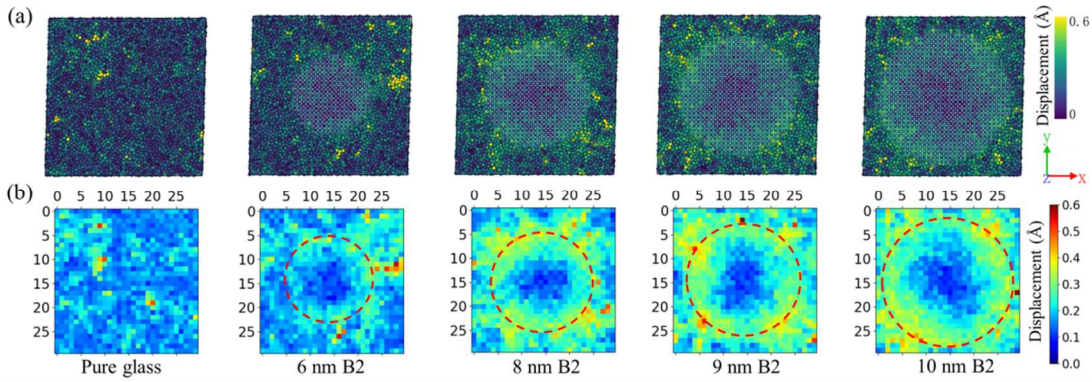

Fig. 11 Non-affine atomic displacements (a) and corresponding heatmaps of non-affine displacements averaged on a 30×30 grid (b) for a pure glass and spherical B2 composites with different B2 sizes shown in a 1 nm thick slice in the middle of the simulation box deformed at 2.5% shear strain.

4 Discussion

4.1 Microstructural effects on complex moduli

The results shown above demonstrate that while storage moduli are mainly dominated by the volumetric effect of mixing hard and soft phases, loss moduli are much more complex and there is no simple relation between the loss modulus and the microstructure of a glass-glass or a glass-crystal composite. First, we have shown in section 2 that not only the density of "hard" icosahedral environments but also their structural heterogeneities (induced here at the glass-glass interfaces) play important roles in the dynamic mechanical responses. A similar situation may also be expected in glasses containing shear bands where the localized deformation strongly rejuvenates the glass, which locally contains a low fraction of icosahedral clusters. Under DMS, shear bands are expected to be prone to irreversible rearrangements, leading to an increased energy dissipation compared to an undeformed glass with a similar average cluster density.

Second, we have shown that the dissipation in crystal-glass composites depends on both the microstructure and loading. When the crystal and the glass phases are forced to deform equally, both the loss and storage moduli result from the volumetric average of the loss and storage moduli in both phases. This point is analyzed quantitatively below. By way of contrast, when the crystal and the glass phases can deform differently, as in the iso-stressed nanolaminate (Fig. 7) or the spherical inclusions (Fig. 10), we have seen that there is a second volumetric effect related to the increased strain amplitude in the glassy matrix, which in turn induces an increased dissipation by triggering an increasing number of plastic events during the deformation cycles. This feature was also reported in the work of Yu et. al [66], who found that mechanical strain has a similar effect as temperature in accelerating the relaxation dynamics. This effect is accompanied by a surface effect related to slipping at the crystal-glass interface, which is analogous to the shear motions seen in the glass-glass interfaces (Fig. 5). This effect is probably present at all temperatures but is difficult to measure below the relaxation peak while Fig. 9 shows a clear evidence of slippage at 1000 K. We therefore believe that such shear motion explains the increased energy dissipation at and above the relaxation peak seen with shear loading, in both the iso-stressed nanolaminate (Fig. 7(b)) and the spherical inclusions (Fig. 10(b)).

The case of spherical inclusions loaded longitudinally is even more intriguing (Fig. 10(a)) since the spherical inclusions hardly affect the low-temperature

dissipation but stabilize the glass phase by shifting the relaxation peak to higher temperatures. It is well-known that a nanoconfinement affects the glass-transition temperature [67,68], but it remains unclear (1) why in our simulations the glass-transition temperature increases while it classically decreases with nanoconfinement and (2) why the relaxation peak temperature varies only with a longitudinal loading and not for instance in shear. From the existing results, we know that the atomic structure of the composite samples as well as the loading condition can influence significantly relaxation behaviors. The volume variation under longitudinal loading and the localized atomic motions near the spherical interface might be key clues to the underlying mechanisms. However, no direct evidence has been found from the atomic trajectory to support these speculations. Despite our best efforts, we have not been able to identify atomistic mechanisms which could explain these observations.

4.2 Dependence on crystalline volume fraction

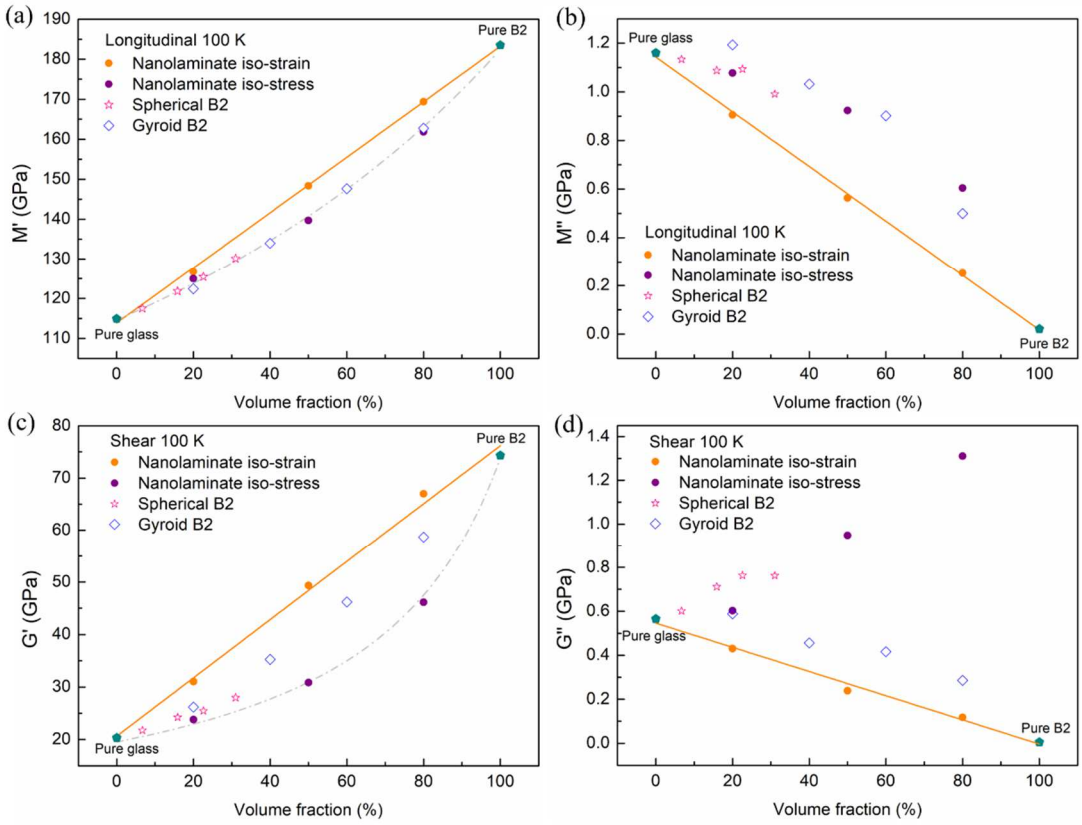

Fig. 12 Relation between complex moduli and volume fraction of B2-CuZr phase for different microstructures (nanolaminates, spherical inclusions and gyroid composites) loaded either longitudinally (a-b) or in shear (c-d).

To explore more quantitatively the low-temperature dependence of the complex moduli on the crystalline phase, the storage and loss moduli were computed at 100 K as function of the volume fraction of B2-CuZr crystal for different microstructures: the nanolaminates and spherical inclusions discussed above, but also interconnected gyroid structures generated with the algorithm proposed in [57] and relaxed using the same protocol as the other composites. The result is shown in Fig. 12. Classical effective modulus calculations [69] yield longitudinal iso-strain and iso-stress moduli for a laminate geometry expressed as

$$M'_{iso-strain} = (1-\phi)M'_a + \phi M'_c \quad (1)$$

and

$$M'_{iso-stress} = \frac{M'_a M'_c}{(1-\phi)M'_c + \phi M'_a} \quad (2)$$

with M'_a (resp. M'_c) the storage modulus of the amorphous (resp. crystal) phase and ϕ, the volume fraction of crystal phase. The same expressions apply for the shear modulus. Note that these expressions reflect only the volumetric effect of mixing phases with different elastic moduli.

In Fig. 12(a) and (c), we recover the linear relationship between M' and G' and the volume fraction ϕ for the iso-strained nanolaminates expected from Eq. (1), as well as the convex relation for the iso-stressed nanolaminates expected from Eq. (2). The same convex curve is followed by the spherical and gyroid composites for longitudinal loading, while in shear, the corresponding G' are in-between $G'_{iso-strain}$ and $G'_{iso-stress}$. This is expected since the iso-strain and iso-stress moduli correspond respectively to the upper bound (Voigt estimation) and lower bound (Reuss estimation) of effective moduli of composites [69]. Storage moduli are therefore simply controlled by the volumetric effect related to the relative fraction of hard and soft phases in the composite.

As discussed above, loss moduli are more intricate. As seen in Fig. 12(b) and (d), for iso-strained nanolaminates, the longitudinal and shear loss moduli ($M''$and G'') follow the same linear relation as in Eq. (1) and thus also result from the volumetric effect of mixing glassy dissipative and crystalline non-dissipative phases. The longitudinal loss modulus M'' of the iso-stress nanolaminate follows a concave shape, which is also followed by the spherical and gyroid B2-CuZr glassy composites. Dissipation is therefore lower than in the pure glass but larger than with the simple volumetric average of Eq. (1). We also see that due to the concave shape of the curve, M'' is close to constant at low volume fractions, which explains why M'' with spherical inclusions does not depend on the sphere radius in Fig. 10(a).

We see a different effect with G'', which is larger in the iso-stressed nanolaminate and spherical composite than in the pure glass. The reason is the sensitivity of G''on the strain amplitude in the glassy phase discussed in Section 3 and illustrated in Fig. 8. This effect is stronger than the simple volumetric effect due to the absence of dissipation in the crystalline phase and leads to an overall increase

of G''. Note that the same confinement effect is not seen with M'' because the storage modulus contrast between the glass and the crystal is smaller for M' than for G', such that the strain in the glassy phase is closer to the overall applied strain with a longitudinal loading than with shear.

5 Conclusions

Dynamic mechanical relaxation has been an important topic in the field of metallic glasses. However, the origin of mechanical relaxation is still far from fully understood. In the current work, MD-DMS simulations in the CuZr metallic glasses and composites with various microstructures were performed to reveal the relaxation characteristics from the atomic scale. We have shown that in a fully glassy system, not only the fraction but also the homogeneity of "hard" icosahedral environments are important. When hard crystalline particles are introduced, the storage modulus simply results from volumetric averages consistent with the classical Voigt and Reuss bounds. Loss moduli are much more complex and depend sensitively on the microstructure and loading condition. In particular, we have seen that while a laminate geometry does not affect the temperature of the relaxation peak, i.e. the glass-transition temperature, but only changes its amplitude, spherical particles can stabilize the glass phase by increasing the temperature of the relaxation peak without affecting its height. Such differentiated nanoconfinement effects deserve a deeper analysis and will be the subject of a future work.

Although the above results are about composites with embedded B2-CuZr crystals, they provide inspiration for understanding the origin of energy dissipation or mechanical relaxation in monolithic metallic glasses. Due to the feature of structural heterogeneities in pure glass, analog to the composites, there are also regions with different moduli, such as "soft regions" and "hard regions", even though without clear boundaries between them. Different regions possess different moduli, and between them there are different strains under cyclic deformation, which induce energy dissipation in the pure glass. Therefore, we can expect for an ideal glass containing absolutely no heterogeneous structure and no imperfection, that there will be no relaxation and energy dissipation. Furthermore, it can be inferred that if there is no shear motion between regions with different moduli, there will still be no energy dissipation. For instance, in the nanolaminates when both phases are deformed with the same strain, there is no shear motion at the glass-crystal interface, which has no effect on energy dissipation. Another evidence in pure glass can also be found in our previous work [48] where the loss modulus derived from the isostatic deformation on the pure $Cu_{64}Zr_{36}$ glass was almost negligible, as expected since no shear exists as the same deformation is applied on three principal directions simultaneously, while for other deformation modes, such as longitudinal deformation, shear or uniaxial deformations, there is shear motion. The above analysis shows that for the energy dissipation or the mechanical relaxation to occur in a pure glass, two conditions must

be met: one is the structural heterogeneity, i.e. the “hard regions” and “soft regions”, with different moduli in different regions, and the other is a local shear deformation, resulting in atomic shear motions between different regions.

Acknowledgements

Simulations were performed using HPC resources from “Fédération Lyonnaise de Modélisation et Sciences Numériques” (FLMSN), partner of EQUIPEX EQUIP@MESO. GJL thanks China Scholarship Council (CSC) for providing a scholarship. YJW and GJL were financially supported by the NSFC (Nos. 12072344 and 11790292), and the Youth Innovation Promotion Association of Chinese Academy of Sciences (No. 2017025).

References

[1] D. Jang, J.R. Greer, Transition from a strong-yet-brittle to a stronger-and-ductile state by size reduction of metallic glasses, Nat. Mater. 9 (2010) 215–219.

[2] H. Choi-Yim, W.L. Johnson, Bulk metallic glass matrix composites, Appl. Phys. Lett. 71 (1997) 3808–3810.

[3] C. Fan, A. Inoue, Improvement of mechanical properties by precipitation of nanoscale compound particles in Zr-Cu-Pd-Al amorphous alloys, Mater. Trans. JIM. 38 (1997) 1040–1046.

[4] J.W. Qiao, H. Jia, P.K. Liaw, Metallic glass matrix composites, Mater. Sci. Eng. R Reports. 100 (2016) 1–69.

[5] R.D. Conner, R.B. Dandliker, W.L. Johnson, Mechanical properties of tungsten and steel fiber reinforced $Zr_{41.25}Ti_{13.75}Cu_{12.5}Ni_{10}Be_{22.5}$ metallic glass matrix composites, Acta Mater. 46 (1998) 6089–6102.

[6] Y. Wang, J. Li, A. V Hamza, T.W. Barbee Jr., Ductile crystalline-amorphous nanolaminates, Proc. Natl. Acad. Sci. U. S. A. 104 (2007) 11155–11160.

[7] F. Szuecs, C.P. Kim, W.L. Johnson, Mechanical properties of $Zr_{56.2}Ti_{13.8}Nb_{5.0}Cu_{6.9}Ni_{5.6}Be_{12.5}$ ductile phase reinforced bulk metallic glass composite, Acta Mater. 49 (2001) 1507–1513.

[8] U. Kühn, J. Eckert, N. Mattern, L. Schultz, ZrNbCuNiAl bulk metallic glass matrix composites containing dendritic bcc phase precipitates, Appl. Phys. Lett. 80 (2002) 2478–2480.

[9] G. He, J. Eckert, W. Löser, L. Schultz, Novel Ti-base nanostructure--dendrite composite with enhanced plasticity, Nat. Mater. 2 (2003) 33–37.

[10] M.L. Lee, Y. Li, C.A. Schuh, Effect of a controlled volume fraction of dendritic phases on tensile and compressive ductility in La-based metallic glass matrix composites, Acta Mater. 52 (2004) 4121–4131.

[11] J. Liu, H. Zhang, H. Fu, Z.-Q. Hu, X. Yuan, In situ spherical B2 CuZr phase reinforced ZrCuNiAlNb bulk metallic glass matrix composite, J. Mater. Res. 25 (2010) 1159–1163.

[12] D.C. Hofmann, J.Y. Suh, A. Wiest, G. Duan, M.L. Lind, M.D. Demetriou, W.L. Johnson, Designing metallic glass matrix composites with high toughness and tensile ductility, Nature. 451 (2008) 1085–1089.
[13] J. Jing, A. Krämer, R. Birringer, H. Gleiter, U. Gonser, Modified atomic structure in a Pd-Fe-Si nanoglass: A Mössbauer study, J. Non. Cryst. Solids. 113 (1989) 167–170.
[14] S. Adibi, Z.D. Sha, P.S. Branicio, S.P. Joshi, Z.S. Liu, Y.W. Zhang, A transition from localized shear banding to homogeneous superplastic flow in nanoglass, Appl. Phys. Lett. 103 (2013) 211905.
[15] X.L. Wang, F. Jiang, H. Hahn, J. Li, H. Gleiter, J. Sun, J.X. Fang, Plasticity of a scandium-based nanoglass, Scr. Mater. 98 (2015) 40–43.
[16] O. Adjaoud, K. Albe, Influence of microstructural features on the plastic deformation behavior of metallic nanoglasses, Acta Mater. 168 (2019) 393–400.
[17] Y.F. Sun, B.C. Wei, Y.R. Wang, W.H. Li, T.L. Cheung, C.H. Shek, Plasticity-improved Zr-Cu-Al bulk metallic glass matrix composites containing martensite phase, Appl. Phys. Lett. 87 (2005) 51905.
[18] J. Das, S. Pauly, C. Duhamel, B.C. Wei, J. Eckert, Microstructure and mechanical properties of slowly cooled $Cu_{47.5}Zr_{47.5}Al_5$, J. Mater. Res. 22 (2007) 326–333.
[19] S. Pauly, G. Liu, G. Wang, U. Kühn, N. Mattern, J. Eckert, Microstructural heterogeneities governing the deformation of $Cu_{47.5}Zr_{47.5}Al_5$ bulk metallic glass composites, Acta Mater. 57 (2009) 5445–5453.
[20] S. Pauly, G. Liu, G. Wang, J. Das, K.B. Kim, U. Kühn, D.H. Kim, J. Eckert, Modeling deformation behavior of Cu--Zr--Al bulk metallic glass matrix composites, Appl. Phys. Lett. 95 (2009) 101906.
[21] Y. Wu, H. Wang, H.H. Wu, Z.Y. Zhang, X.D. Hui, G.L. Chen, D. Ma, X.L. Wang, Z.P. Lu, Formation of Cu–Zr–Al bulk metallic glass composites with improved tensile properties, Acta Mater. 59 (2011) 2928–2936.
[22] D. Şopu, M. Stoica, J. Eckert, Deformation behavior of metallic glass composites reinforced with shape memory nanowires studied via molecular dynamics simulations, Appl. Phys. Lett. 106 (2015) 211902.
[23] M. Sepulveda-Macias, N. Amigo, G. Gutierrez, Tensile behavior of $Cu_{50}Zr_{50}$ metallic glass nanowire with a B2 crystalline precipitate, Phys. B Condens. Matter. 531 (2018) 64–69.
[24] D. Şopu, K. Albe, J. Eckert, Metallic glass nanolaminates with shape memory alloys, Acta Mater. 159 (2018) 344–351.
[25] N. Amigo, M. Sepulveda-Macias, G. Gutierrez, Enhancement of mechanical properties of metallic glass nanolaminates via martensitic transformation: Atomistic deformation mechanism, Mater. Chem. Phys. 225 (2019) 159–168.
[26] S. Pauly, J. Das, J. Bednarcik, N. Mattern, K.B. Kim, D.H. Kim, J. Eckert, Deformation-induced martensitic transformation in Cu-Zr-(Al, Ti) bulk metallic glass composites, Scr. Mater. 60 (2009) 431–434.

[27] Y. Wu, Y. Xiao, G. Chen, C.T. Liu, Z. Lu, Bulk metallic glass composites with transformation-mediated work-hardening and ductility, Adv. Mater. 22 (2010) 2770–2773.
[28] K.K. Song, S. Pauly, Y. Zhang, P. Gargarella, R. Li, N.S. Barekar, U. Kühn, M. Stoica, J. Eckert, Strategy for pinpointing the formation of B2 CuZr in metastable CuZr-based shape memory alloys, Acta Mater. 59 (2011) 6620–6630.
[29] C.A. Angell, K.L. Ngai, G.B. McKenna, P.F. McMillan, S.W. Martin, Relaxation in glassforming liquids and amorphous solids, J. Appl. Phys. 88 (2000) 3113–3157.
[30] L. Berthier, G. Biroli, Theoretical perspective on the glass transition and amorphous materials, Rev. Mod. Phys. 83 (2011) 587–645.
[31] J.C. Qiao, Q. Wang, J.M. Pelletier, H. Kato, R. Casalini, D. Crespo, E. Pineda, Y. Yao, Y. Yang, Structural heterogeneities and mechanical behavior of amorphous alloys, Prog. Mater. Sci. (2019) 250–329.
[32] W.H. Wang, Dynamic relaxations and relaxation-property relationships in metallic glasses, Prog. Mater. Sci. 106 (2019) 100561.
[33] J.C. Qiao, J.-M. Pelletier, Dynamic universal characteristic of the main α relaxation in bulk metallic glasses, J. Alloys Compd. 589 (2014) 263–270.
[34] H.B. Yu, K. Samwer, Atomic mechanism of internal friction in a model metallic glass, Phys. Rev. B. 90 (2014) 144201.
[35] H.B. Yu, W.H. Wang, H.Y. Bai, Y. Wu, M.W. Chen, Relating activation of shear transformation zones to β relaxations in metallic glasses, Phys. Rev. B. 81 (2010) 220201.
[36] H.B. Yu, W.H. Wang, K. Samwer, The β relaxation in metallic glasses: an overview, Mater. Today. 16 (2013) 183–191.
[37] Z. Wang, B.A. Sun, H.Y. Bai, W.H. Wang, Evolution of hidden localized flow during glass-to-liquid transition in metallic glass, Nat. Commun. 5 (2014) 6823.
[38] H.B. Yu, R. Richert, K. Samwer, Structural rearrangements governing Johari-Goldstein relaxations in metallic glasses., Sci. Adv. 3 (2017) e1701577.
[39] H.B. Yu, M.H. Yang, Y. Sun, F. Zhang, J.B. Liu, C.-Z. Wang, K.-M. Ho, R. Richert, K. Samwer, Fundamental link between β relaxation, excess wings, and cage-breaking in metallic glasses, J. Phys. Chem. Lett. 9 (2018) 5877–5883.
[40] S. Küchemann, R. Maaß, Gamma relaxation in bulk metallic glasses, Scr. Mater. 137 (2017) 5–8.
[41] Y. Sun, S. Peng, Q. Yang, F. Zhang, M. Yang, C. Wang, K. Ho, H. Yu, Predicting Complex Relaxation Processes in Metallic Glass, Phys. Rev. Lett. 123 (2019) 105701.
[42] J. Kong, Z.T. Ye, W. Chen, X.L. Shao, K.H. Wang, Q. Zhou, Dynamic mechanical behavior of a Zr-based bulk metallic glass composite, Mater. Des. 88 (2015) 69–74.
[43] J.C. Qiao, B.A. Sun, J. Gu, M. Song, J.M. Pelletier, J.W. Qiao, Y. Yao, Y. Yang, Abnormal internal friction in the in-situ $Ti_{60}Zr_{15}V_{10}Cu_5Be_{10}$ metallic glass matrix composite, J. Alloys Compd. 724 (2017) 921–931.

[44] G.J. Lyu, J.C. Qiao, J. Gu, M. Song, J.-M. Pelletier, Y. Yao, Experimental analysis to the structural relaxation of $Ti_{48}Zr_{20}V_{12}Cu_5Be_{15}$ metallic glass matrix composite, J. Alloys Compd. 769 (2018) 443–452.

[45] J.C. Qiao, T.P. Ren, G.J. Lyu, L. Zhang, H.F. Zhang, J.M. Pelletier, Y. Yao, Physical mechanism of internal friction behavior of β-type bulk metallic glass composites, Mater. Sci. Eng. A. 739 (2019) 193–197.

[46] H.T. Jeong, W. Yook, B.J. Kim, W.T. Kim, D.H. Kim, Dynamic mechanical properties of a dual-phase $Zr_{28}Y_{28}Al_{22}Co_{22}$ metallic glass, Met. Mater. Int. 16 (2010) 517–522.

[47] G.J. Lyu, J.C. Qiao, J.M. Pelletier, Y. Yao, The dynamic mechanical characteristics of Zr-based bulk metallic glasses and composites, Mater. Sci. Eng. A. 711 (2018) 356–363.

[48] G.J. Lyu, J.C. Qiao, Y. Yao, J.M. Pelletier, D. Rodney, J. Morthomas, C. Fusco, Dynamic correspondence principle in the viscoelasticity of metallic glasses, Scr. Mater. 174 (2020) 39–43.

[49] B. Wang, Z.Y. Zhou, P.F. Guan, H.B. Yu, W.H. Wang, K.L. Ngai, Invariance of the relation between α relaxation and β relaxation in metallic glasses to variations of pressure and temperature, Phys. Rev. B. 102 (2020) 1–9.

[50] S. Plimpton, Fast parallel algorithms for short-range molecular dynamics, J. Comput. Phys. 117 (1995) 1–19.

[51] V. Borovikov, M.I. Mendelev, A.H. King, Effects of stable and unstable stacking fault energy on dislocation nucleation in nano-crystalline metals, Model. Simul. Mater. Sci. Eng. 24 (2016) 85017.

[52] D. Şopu, F. Moitzi, N. Mousseau, J. Eckert, An atomic-level perspective of shear band formation and interaction in monolithic metallic glasses, Appl. Mater. Today. 21 (2020) 100828.

[53] X. Yuan, D. Şopu, F. Moitzi, K.K. Song, J. Eckert, Intrinsic and extrinsic effects on the brittle-to-ductile transition in metallic glasses, J. Appl. Phys. 128 (2020) 125102.

[54] P. Wang, X. Yang, Atomistic investigation of aging and rejuvenation in CuZr metallic glass under cyclic loading, Comput. Mater. Sci. 185 (2020) 109965.

[55] A. Stukowski, Visualization and analysis of atomistic simulation data with OVITO-the Open Visualization Tool, Model. Simul. Mater. Sci. Eng. 18 (2010) 015012.

[56] P.M. Derlet, R. Maaß, Emergent structural length scales in a model binary glass - The micro-second molecular dynamics time-scale regime, J. Alloys Compd. 821 (2020) 153209.

[57] D.J. Yoo, Computer-aided porous scaffold design for tissue engineering using triply periodic minimal surfaces, Int. J. Precis. Eng. Manuf. 12 (2011) 61–71.

[58] Z.D. Sha, P.S. Branicio, Q.X. Pei, Z.S. Liu, H.P. Lee, T.E. Tay, T.J. Wang, Strong and superplastic nanoglass, Nanoscale. 7 (2015) 17404–17409.

[59] A.J. Cao, Y.Q. Cheng, E. Ma, Structural processes that initiate shear localization in metallic glass, Acta Mater. 57 (2009) 5146–5155.

[60] Y.Q. Cheng, E. Ma, Atomic-level structure and structure–property relationship in metallic glasses, Prog. Mater. Sci. 56 (2011) 379–473.
[61] J. Ding, Y.Q. Cheng, E. Ma, Full icosahedra dominate local order in $Cu_{64}Zr_{34}$ metallic glass and supercooled liquid, Acta Mater. 69 (2014) 343–354.
[62] B. Wang, B.S. Shang, X.Q. Gao, W.H. Wang, H.Y. Bai, M.X. Pan, P.F. Guan, Understanding Atomic-Scale Features of Low Temperature-Relaxation Dynamics in Metallic Glasses, J. Phys. Chem. Lett. 7 (2016) 4945–4950.
[63] N. Wang, J. Ding, F. Yan, M. Asta, R.O. Ritchie, L. Li, Spatial correlation of elastic heterogeneity tunes the deformation behavior of metallic glasses, Npj Comput. Mater. 4 (2018) 1–10.
[64] B. Wang, L. Luo, E. Guo, Y. Su, M. Wang, R.O. Ritchie, F. Dong, L. Wang, J. Guo, H. Fu, Nanometer-scale gradient atomic packing structure surrounding soft spots in metallic glasses, Npj Comput. Mater. 4 (2018) 41.
[65] E. Ma, Tuning order in disorder, Nat. Mater. 14 (2015) 547–552.
[66] H.B. Yu, R. Richert, R. Maaß, K. Samwer, Strain induced fragility transition in metallic glass, Nat. Commun. 6 (2015) 1–6.
[67] C.L. Jackson, G.B. McKenna, The glass transition of organic liquids confined to small pores, J. Non. Cryst. Solids. 131–133 (1991) 221–224.
[68] C.J. Ellison, J.M. Torkelson, The distribution of glass-transition temperatures in nanoscopically confined glass formers, Nat. Mater. 2 (2003) 695–700.
[69] R. Hill, The elastic behaviour of a crystalline aggregate, Proc. Phys. Soc. Sect. A. 65 (1952) 349–354.

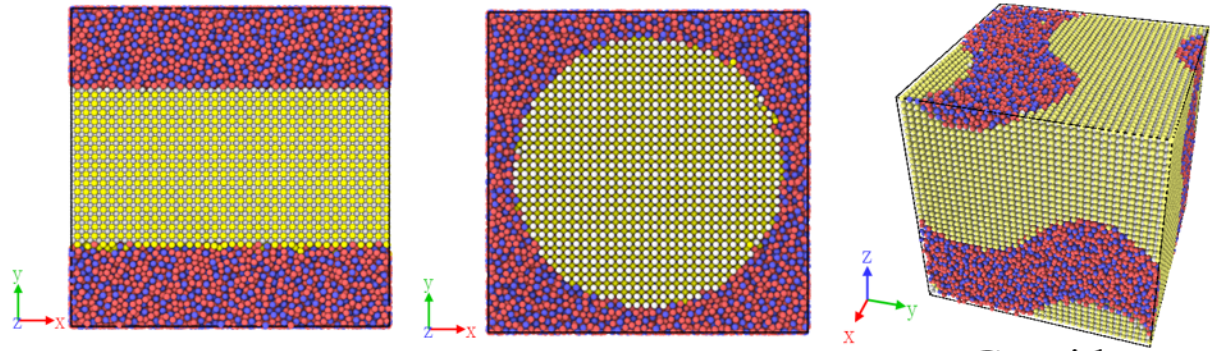
Nanolaminate
Spherical
Gyroid

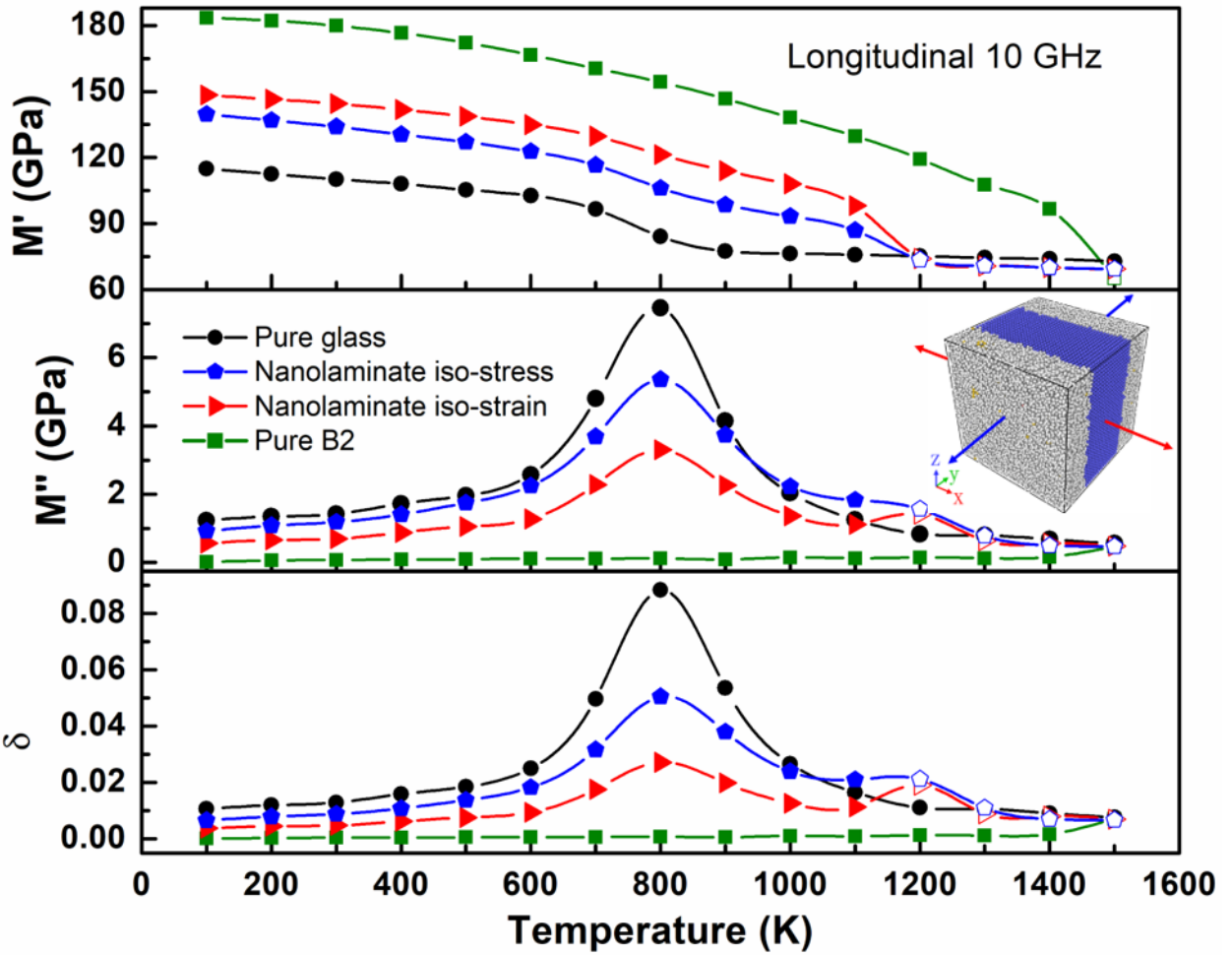
Longitudinal 10 GHz
M' (GPa)
M'' (GPa)
δ
Pure glass
Nanolaminate iso-stress
Nanolaminate iso-strain
Pure B2
Temperature (K)